ISSN 0001-4338, Izvestiya, Atmospheric and Oceanic Physics, 2024, Vol. 60, No. 5, pp. 533–543. © Pleiades Publishing, Ltd., 2024.

Technique for Determining Tropospheric Ozone Content from Spectral Measurements of Outgoing Thermal Radiation by the IKFS-2 Satellite Instrument

A. V. Polyakov[a, *], Ya. A. Virolainen[a], G. M. Nerobelov[a, b, c], and S. V. Akishina[a]

[a] *St. Petersburg State University, St. Petersburg, 199034 Russia*

[b] *St. Petersburg Federal Research Center, Russian Academy of Sciences, Research Center for Environmental Safety, Russian Academy of Sciences, St. Petersburg, 187110 Russia*

[c] *Russian State Hydrometeorological University, St. Petersburg, 195196 Russia*

**e-mail: a.v.polyakov@spbu.ru*

Received March 19, 2024; revised May 20, 2024; accepted July 10, 2024

Abstract—A technique for determining the tropospheric ozone (TO) content from the spectra of outgoing thermal infrared (IR) radiation based on the principal component method and neural network approach is proposed. To train the artificial neural networks, TO data calculated from ozone profiles of vertical ozone content derived from ozonesondes are used. The TCO is considered the ozone content in the atmospheric layers from the earth's surface to pressure levels of 400 and 300 hPa. The error of approximating TO values on training data is 2.7 and 3.6 DU for layers below 400 and 300 hPa, respectively. The methodology is validated on the basis of comparison with ground-based TO measurements at the NDACC international observing network of stations using solar infrared spectra. The mean standard deviations of the differences between the ground-based infrared measurements at 19 stations and the derived TO values from the IKFS-2 data were about 3 DU. The mean differences depend on the altitude and geographical location of the ground station, varying from +3 to −12 DU. The discrepancies between the ground-based measurements and satellite data correspond to the results of other authors obtained for the IASI satellite instrument, which is close in characteristics. The paper presents examples of the global distribution of mean monthly TO values for different seasons.

Keywords: tropospheric ozone, remote sensing of the atmosphere, IKFS-2

DOI: 10.1134/S000143382470049X

INTRODUCTION

Attention to tropospheric ozone (TO) has recently increased for a number of reasons. First, ozone participates in chemical and photochemical processes, determining the oxidizing capacity of the troposphere. Entering the body through the respiratory tract, tropospheric ozone negatively affects the health of people and animals (Stanek et al., 2011). According to (Amann et al., 2008), elevated values of ground-level ozone (GLO) exceeding maximum permissible concentrations cause more than 20 000 deaths in 25 European Union countries annually. Ozone also has a negative effect on vegetation (Mills et al., 2018). Second, tropospheric ozone is one of the main greenhouse gases affecting the radiation balance and climate change of the earth (Zvyagintsev, 2013). By absorbing the earth's thermal radiation in the infrared region of the spectrum, ozone contributes to the greenhouse effect. According to the IPCC report for 2021 (Forster et al., 2021), the contribution of tropospheric ozone to the total anthropogenic impact on the planet's radiation balance is 4–20%, which is consistent with earlier data (Karol et al., 2012). The models estimate the magnitude of the TO radiative forcing to be $+(0.40 \pm 0.20)$ W m^{-2} (*IPCC*, 2013). The large scatter in estimates of the contribution of TO to the radiative forcing is caused, in particular, by insufficient knowledge about the spatial distribution of TO (Wu et al., 2007).

The main sources of ozone in the troposphere are the supply of ozone from the stratosphere and the formation as a result of photochemical reactions. The power of the second source is an order of magnitude higher than the first (Young et al., 2013), but most of the ozone formed during photochemical reactions is destroyed or deposited on the earth's surface, as a result of which, on average, both sources make approximately the same contribution. In different seasons and in different regions, the relative contribution of sources can vary significantly depending on the emissions of ozone precursors (NO_x, CO, CH_4, OH, anthropogenic, and biogenic volatile compounds) and meteorological conditions (Karol et al., 2012; Zvyagintsev, 2013), which leads to significant variability in TO.

The results of regular monitoring of both GLO and TO have been collected for about 10 years within the framework of the international TOAR project (Tropospheric Ozone Assessment Report) (https://toar-data.org). Monitoring includes an integrated approach consisting of ground-based local and remote measurements, aircraft, satellite observations, etc. The first measurements of GLO began in the 1870s; in the 1930s–1940s, ozonesonde launches began, which gave an idea of the ozone content throughout the troposphere (Tarasick et al., 2019). In 1960–1970, the widespread study of GLO and vertical ozone profiles began. The WOUDC database (https://woudc.org/home.php) presents data from several dozen ground stations that launch ozonesondes, the measurement accuracy of which has recently increased, which makes it possible to use their data for the validation of satellite measurements (Tarasick et al., 2021). At individual ground stations, TO (vertical profiles) is measured periodically or during measurement campaigns using the lidar method and the Umkehr inversion method using Brewer and Dobson spectrophotometers (Gaudel et al., 2018). In addition, TO on cloudless days is obtained at stations of the IRWG-NDACC international measurement network (InfraRed Working Group of Network for the Detection of Atmospheric Composition Change) (https://www2.acom.ucar.edu/irwg), equipped with Fourier spectrometers (FS) high spectral resolution—FTIR measurements (Fourier Transform InfraRed) (Vigouroux et al., 2015). Ground-based measurements are used both to investigate local changes in TO and validate satellite measurements and tune numerical atmospheric models at the regional scale.

In Russia, there is a ground-based network for monitoring GLO under background conditions, which includes about 20 stations in 13 regions of the country, equipped with modern gas analyzers (Andreev et al., 2023). In addition, Russia periodically conducts experiments to determine TO, covering large areas, for example, aircraft measurements in the Siberian region (Antokhin et al., 2013) and over all seas of the Russian sector of the Arctic (Belan et al., 2022), as well as transcontinental measurements of atmospheric composition on the TROICA mobile railway laboratory (Elansky et al., 2021). Vertical ozone profiles in the upper troposphere are occasionally measured using lidars (Matvienko et al., 2019) and ozonesondes (Dorokhov et al., 2013). At the NDACC station in St. Petersburg, on the campus of St. Petersburg State University in Peterhof, regular TO measurements have been carried out since 2009 using a Bruker IFS 125HR FS (Virolainen et al., 2023a).

Currently, global information on TO is regularly obtained using the IASI (Dufour et al., 2012) and TROPOMI (Hubert et al., 2021) satellite instruments, as well as joint measurements by the IASI and GOME-2 instruments (Cuesta et al., 2013), OMI and MLS (Ziemke et al., 2006), etc. It should be noted that instruments such as OMI, GOME-2, TROPOMI, etc., using measurements of solar radiation, have certain gaps in data; for example, there are absolutely no TO measurements under polar (and normal) night conditions. The most complete global coverage of TO measurements is provided by satellite instruments using their own thermal radiation. In recent years, such measurements have been carried out only by the IASI satellite instrument.

To validate satellite TO measurements, both ozone sounding data and various ground-based measurements are typically used. The work (Dufour et al., 2012) analyzed the determination of TO from spectroscopic measurements of the IASI satellite instrument in 2008 using two algorithms for solving the inverse problem, IASI_LATMOS and IASI_LISA. On average, for all comparisons in midlatitudes (320 days of comparisons), the mean differences (MDs) between satellite and ozonesonde measurements were +0.6 DU with standard deviations of differences (SDD) of 5.5 DU (IASI_LATMOS) and +1.0 DU with SDD in 6.1 DU (IASI_LISA). In (Boynard et al., 2018), measurements of TO IASI_LATMOS for 2008–2017 were compared with ozone sounding data at 56 stations and FTIR measurements at 6 stations of the IRWG-NDACC network. MDs for NDACC-IRWG stations varied from –4 to +0.5 DU; SDD was 2.5–3.9 unit. In (Cuesta et al., 2013), information on the ozone content, including in the troposphere, was obtained from data from joint measurements by the IASI and GOME-2 instruments. The results were compared with ozonesonde data for the summer of 2009 at ten European stations. The MD (SDD) was 0.01 DU (4.3 DU) for ozone content in the 0–6 km layer and –0.73 DU (6.2 DU) for ozone content in the 0–12 km layer. In (Virolainen et al., 2023b), IASI_LATMOS and IASI_LISA satellite measurement data for 2009–2021 and IASI-GOME2 for 2016–2021 in the 0–8 km tropospheric layer were compared with FTIR measurement data at the IRWG-NDACC St. Petersburg station; in (Virolainen et al., 2023), these comparisons were also extended to two other IRWG-NDACC stations: Kiruna and Izaña. It was shown that the SDDs between satellite and ground-based TO measurements are within the total measurement errors of the compared data for the IASI_LATMOS (9–13%) and IASI_LISA (12–16%) algorithms, while the MDs with the IASI-GOME2 satellite data exceed the errors individual measurements, amounting to 16–22%. In addition, for the Izaña station, a statistically significant drift (about –12% per decade) was detected in satellite TO measurements by the IASI instrument for 2012–2021.

Note that in Russia there are currently no satellite methods for measuring TO. The proposed work solves the problem of creating a methodology for determining TO from spectra measured by the IKFS-2 device (Golovin et al., 2014), which is part of the equipment on meteorological spacecraft of the Meteor-M series no. 2 (Asmus et al., 2014). The measured spectra

include 2701 spectral channels with an apodized spectral resolution of 0.7 cm^{-1} in the spectral range 660–1210 cm^{-1} and 1.4 cm^{-1} in the region 1210–2000 cm^{-1}. The first spacecraft of this series supplied data from the beginning of 2015 to the end of 2022; Meteor M spacecraft no. 2-4 is currently in orbit. In order to study the ozone content only in the troposphere layer, in this work we consider TO to be the ozone content in layers from the surface to a level with atmospheric pressure less than 300 and 400 hPa, which approximately corresponds to layers limited from above by heights of 9 and 7 km, respectively. Below we use all available IKFS-2 spectral data for 2015–2022, both for artificial neural network (ANN) training and validation.

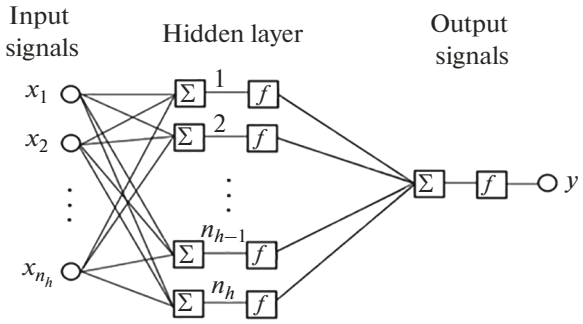

Fig. 1. Three-layer perceptron. The first layer is considered to be the input signal sources, followed by the so-called hidden layer, then the third layer of output signals.

METHODS

Approach and Methodology

To solve the inverse problem of determining TO, we used an approach previously successfully applied to determine the total ozone content (TOC) in the atmosphere from the spectra of outgoing thermal IR radiation measured by the IKFS-2 device (Garkusha et al. 2017, Polyakov et al. 2021, 2023, Timofeyev et al. 2019). Namely, based on independent data on TO, calculated from vertical ozone profiles obtained by ozonesondes, and matched to them by location and time of measurements of the IKFS-2 spectra, an ANN was trained (an approximation of the dependence of TO on a set of predictors in ANN form) that made it possible to determine TO from IKFS-2 spectra.

As a first approximation, we completely repeated the previously developed method for TOC, only replacing TOC with TO. Namely, one of the simplest ANN configurations was used: a three-layer perceptron (Fig. 1).

Mathematically, this ANN is represented by expression (1):

$$y = f\left(b^2 + \sum_{i=1}^{N_h} \omega_i^2 f\left(b_i^1 + \sum_{j=1}^{N} \omega_{i,j}^1 x_j\right)\right). \quad (1)$$

Here, f is the activation function; $\vec{X} = \{x_j\}$ is the vector of input parameters; and $b_i^1, \omega_{i,j}^1, \omega_i^2$, and b^2 are coefficients.

ANN training means minimizing the root mean square error σ_{app} approximation of training set data by coefficients $b_i^1, \omega_{i,j}^1, \omega_i^2$, and b^2 (2)

$$\sigma_{app} = \sqrt{\frac{\sum_S \left(Y_s - y\left(\vec{X_s}\right)\right)^2}{\sum_S 1}} \to \min, \quad (2)$$

where set of couples $\{\vec{X}, Y\}_s$ is the training data set. The minimum error provides the best closeness in the root-mean-square sense to the actual TO values $\{Y\}_s$ and obtained using the mathematical algorithm ANN (1), which allows one to select the optimal values of the coefficients. Test and validation datasets are used to monitor network overtraining and to optimize the ANN structure. An increase in the approximation error using such testing data sets is a sign of network adaptation only to the training data set. We emphasize that we did not use the program libraries that have become widespread in recent years for working with ANN TensorFlow and Keras. All calculations were performed using original software developed earlier (Polyakov et al., 2014a, 2014b) both for training the ANN and for calculations on it.

Following previous experience in solving the inverse problem with respect to TOC, we used the satellite zenith angle (the angle between the normal to the surface and the direction to the satellite at the center of the observation pixel), the latitude of the measurement pixel, the day of the year, and the principal components (PCs) as predictors of two spectrum sections in the IKFS-2 measurement area: 660–1210 and 980–1080 cm^{-1}. The first of these spectral intervals carries information about the general state of the atmosphere and surface: temperature profile, surface temperature and emissivity, humidity profile, etc., while the second, containing the ozone absorption band, allows one to isolate information related directly to ozone.

ANN Training

To train the ANN, we used the integral gas content in the layer below 300 hPa or below 400 hPa, calculated based on vertical ozone profiles measured by ozonesondes.

It should be noted that, although in the presence of continuous clouds, complete information about TO is not contained in the spectra due to the shielding of IR radiation by the cloud, the possibility of estimating TO in partial clouds may be available, depending on the intensity of the clouds and the height of its upper boundary. Therefore, when training the ANN, we considered cloudless situations (for the cloud detec-

Table 1. Approximation errors for different training sets

1	Textbook	Number of textbook pairs	Number of validation set pairs	Textbook approximation error	Validation set approximation error
	Upper limit TO 300 hPa				
2	Ozonesondes, all spectra, 12 h 100 km	42821	14184	4.49	4.95
2a	Ozonesondes, all spectra, 12 h, 100 km, p0	42821	14184	3.49	3.70
3	Ozonesondes, cloudless, 12 h 100 km	13126	4315	3.42	5.29
4	Ozonesondes, all spectra, 24 h 200 km	341274	113418	5.19	5.30
5	Ozonesondes, cloudless, 24 h 200 km	102279	34263	4.77	5.09
	Upper limit TO 400 hPa				
6	Ozonesondes, all spectra, 24 h 200 km	341537	113526	4.05	4.18
7	Ozonesondes, all spectra, 24 h 200 km No latitude and season	341537	113526	4.43	4.47

p0, surface pressure used in the set of predictors instead of the latitude of the observation point.

tion algorithm, see (Rublev et al., 2004, Asmus et al., 2017)), as well as all IKFS-2 measurements. The predictors, as mentioned above, include the PCs of the spectrum in two spectral intervals, the zenith angle of the satellite, the latitude of the observation pixel, and the day of the year. Note that the entire resulting set of measurement pairs was divided into three sets: textbook (60%) and test and validation sets (20% each).

Training was performed for up to 100 epochs, and at each epoch, the cost function (also known as the approximation error), equal to the root-mean-square difference between independently measured and estimated TO values using ANN, was minimized using up to 100 steps of the Fletcher–Reeve method and up to 200 steps of the Davidson–Fletcher–Paella method. Minimization programs are taken from the open access MSU program library (http://num-anal.srcc.msu.ru/lib_na/cat/mn/mnb3r.htm, mnb4d.htm). We considered several training datasets and a variant of ANN in which the latitude and day of year of measurements were not included in the predictors. The sets varied depending on the values of temporal and spatial data mismatch in the pair. To select pairs, mismatch values of 12 and 24 h were considered by time and, by spatial measurement point, 100 and 200 km. Table 1 shows the approximation errors of the decision operator for the considered data sets and ANN. The "all spectra" entry means IKFS-2 spectra measured under both cloudy and cloudless conditions.

As can be seen from rows 2 and 2a (with selection parameters of 12 h and 100 km) and, to a greater extent, 3 (cloudless selection) of Table 1, in the case of ozonesondes, slight overfitting is observed (the approximation error for the validation data set is noticeably larger than the error for the training set). Although there are techniques that allow you to train an ANN in this situation, the best way to avoid overtraining is to increase the size of the tutorial. To do this, consider the selection option for 24 h and 200 km, shown in lines 4 and 5 of Table 1. Although we observe an increase in the approximation error in these cases compared to lines 2 and 3, we should expect better results from these options in validation due to the increase in the size of the textbook.

Line 2a shows a variant of the predictor set in which surface pressure p0 is used instead of latitude. During training, this is the pressure at the probe launch site; when solving the inverse problem, this is the pressure at the device's aiming pixel according to NCEP GFS data. As you can see, the effect is insignificant, although, interestingly, the approximation error on the validation set decreased slightly (by 0.13 DU). In our opinion, this may indicate a more physical set of predictors in this case.

Line 7 describes a data set that does not include latitude and day of year information. A comparison of rows 6 and 7 shows that using latitude and fraction of a year noticeably reduces the discrepancy. Namely, the textbook approximation error when excluding these parameters from the list of predictors leads to an increase in the approximation error by approximately 10% (4.43 instead of 4.05).

Thus, an analysis of Table 1 allowed us to focus on the training option for further research: (1) for all situations, including cloudy ones; (2) the set of predictors includes, in addition to PC spectra, the satellite zenith angle, latitude, and day of year; and (3) mismatch values in data pairs of 200 km in space and 24 h in time are acceptable. Next, we optimized the ANN structure by selecting, based on the results of a series of calculations, the optimal number of PCs included in the set of predictors and the number of hidden layer neurons (HLN); see Table 2.

Taking as a basis the ANN variant used earlier in the works of (Garkusha et al., 2017, Polyakov et al., 2021) when determining TOC with 25 PCs of the entire

Table 2. Selection of the optimal ANN structure; 200 optimization epochs, tropospheric layer height 400 hPa. The ANN circuit designation indicates the composition of the ANN input parameter vector. The first number represents the PC number of the entire spectrum, the second the PC number of the ozone band, and the third the HLN number. Approximation errors are given in DU

No.	ANN scheme	Number of ANN coefficients	Textbook approximation error	Test set approximation error	Validation set approximation error
1	25-50-40	3201	2.77	2.80	2.79
2	25-10-40	1601	2.78	2.80	2.79
3	25-0-40	1201	2.82	2.83	2.82
4	30-0-40	1401	2.80	2.80	2.80
5	35-0-40	1601	2.78	2.80	2.79
6	**50-0-60**	**3301**	**2.72**	**2.74**	**2.74**
7	50-0-50	2751	2.73	2.75	2.75
8	50-0-40	2201	2.75	2.76	2.77
9	40-0-60	2701	2.71	2.73	2.73
10	35-0-60	2401	2.71	2.73	2.72
11	40-0-50	2251	2.74	2.76	2.76
12	30-0-60	2101	2.72	2.74	2.74
13	40-0-70	3151	2.70	2.73	2.73
14	35-0-65	2601	2.70	2.72	2.72
15	**35-0-55**	**2201**	**2.72**	**2.74**	**2.74**

spectrum, 50 PCs of the ozone band, and 40 HLNs among the predictors, we tried to reduce the number of PCs of the ozone band. The results are shown in lines 1–5. It can be seen that, when the PC number of the ozone band is reduced to 10, the approximation error σ_{app} (approximation error (AE)) practically did not change (line 2), but when this amount decreases to 0, an increase in AE by 0.03–0.04 DU is observed for all three subsamples. To compensate for this growth, we will increase the number of PCs across the entire spectrum. As one can see, an increase in this amount by 5 (line 4) does not provide full compensation, but an increase by 10 almost completely compensates for the cancellation of the use of the PC ozone band (line 5). Therefore, further we consider options without using a PC ozone strip. For a number of obvious reasons, it is desirable to use the simplest possible ANN structure with a minimum number of coefficients determined during training. To do this, we will consider several ANN options and choose the option that is optimal from the point of view of the combination of a small approximation error and a small number of determined coefficients.

As a deliberately redundant ANN option, consider the option with 50 PCs and 60 HLNs (line 6). As can be seen, the AE relative to the main option decreased by 0.05–0.06 DU for all three subsamples. Below in lines 7–15, we varied the number of PCs and HLNs by analyzing the AE. Based on this analysis, we chose line 15 for further work: 35 PC spectrum and 55 HLN.

The selection of the ANN structure was performed for the atmospheric layer below 400 hPa. To verify the suitability of the same choice for the layer below 300 hPa, we compare in Table 3 the AE for the selected and redundant ANN schemes. Since the choice of the upper boundary of the layer under consideration is related to the latitudinal zone, we will perform these comparisons both for all latitudes and excluding polar and close latitudes for the belt 60° S–60° N.

Table 3 shows that the increase in AE when moving from the redundant to the chosen scheme does not exceed 0.07 DU on the training data set and 0.03–0.04 DU on the test and validation sets, which allows us to conclude that the selected ANN configuration is suitable for the atmospheric layer below 300 hPa.

RESULTS AND DISCUSSION

Comparison with Ground-Based FTIR Measurement Data

We used the resulting ANNs to process IKFS-2 measurements near ground stations of the IRWG-NDACC network equipped with a Bruker IFS 125HR high spectral resolution FS, measuring the spectra of direct solar IR radiation in a cloudless atmosphere or in large cloud breaks. This allowed us to compare the TO values obtained using our technique with data from independent FTIR measurements (https://www-air.larc.nasa.gov/missions/ndacc/data.html). Geographical coordinates and heights of stations above sea level are shown in Table 4. In the last column of

Table 3. AE for two ANN structures for all latitudes and mid- and tropical latitudes. The upper limit of the calculation is TO 300 hPa

No.	ANN scheme	Number of ANN coefficients	Textbook approximation error	Test set approximation error	Validation set approximation error
200 epochs, all latitudes					
1	50-0-60	3301	3.66	3.73	3.72
2	35-0-55	2201	3.69	3.76	3.75
200 epochs, latitude belt 60° S–60° N					
4	35-0-55	2201	3.56	3.62	3.64
5	50-0-60	3301	3.50	3.60	3.60

Table 4. Geographic coordinates and altitudes above sea level at the IRWG-NDACC station

	Station	Latitude	Longitude	Altitude	Notes
1	Eureka, Canada	80.05° N	86.42° W	610 m	Glacier
2	Ny Ålesund, Norway	78.92° N	11.93° E	15 m	Island
3	Thule (Greenland), Denmark	76.53° N	68.74° W	220 m	Glacier
4	Kiruna, Sweden	67.84° N	20.41° E	419 m	
5	Harestua, Norway	60.2° N	10.8° E	596 m	
6	St. Petersburg, Russia	59.9° N	29.8° E	20 m	
7	Bremen, Germany	53.1° N	8.8° E	27 m	
8	Zugspitze, Germany	47.42° N	10.98° E	2964 m	Mountains
9	Jungfraujoch, Switzerland	46.55° N	7.98° E	3580 m	Mountains
10	Toronto TAO, Canada	43.66° N	79.40° W	174 m	
11	Rikubetsu, Japan	43.46° N	143.77° E	380 m	Island
12	Boulder (Colorado), United States	39.99° N	105.26° W	1634 m	Mountains
13	Tsukuba, Japan	36.05° N	140.13° E	31 m	Island
14	Izaña (Tenerife), Spain	28.30° N	16.48° W	2367 m	Small island
15	Mauna Loa (Hawaii), United States	19.54° N	155.58° W	3397 m	Small island
16	Altzomoni, Mexico	19.12° N	98.66° W	3985 m	Mountains
17	Maido (Réunion), France	21.1° S	55.4° E	2155 m	Small island
18	Wollongong, Australia	34.41° S	150.88° E	30 m	
19	Lauder, New Zealand	45.04° S	169.68° E	370 m	Island

Table 4, there are some features of the location of stations that can affect the results of comparison with satellite measurement data. For example, for comparison with ground-based measurements, daily averaged satellite measurements within a radius of 200 km from ground stations were taken into account; i.e., when a station is located in a mountainous area, some of the satellite data may cover both mountains and lowlands, and when the station is located on islands, most of the satellite measurements may relate to the water surface, and not to the station itself.

As can be seen from Table 4, all but three stations are located in the Northern Hemisphere. Among them, seven stations are located in Europe, five in North America, two in Japan, and two on the islands. There are five stations in high latitudes, ten in middle latitudes, and four in tropical latitudes. Thus, the FTIR measurements under consideration cover all latitude zones from the middle latitudes of the Southern Hemisphere to the high latitudes of the Northern Hemisphere.

To confirm the validity of the choice of the number of PCs and HLNs, we performed comparisons of satellite TO measurements obtained under different variants of the ANN structure with the FTIR measurement data. These comparisons with independent data allow for more informed choices about network structure than AE analysis. The results of comparisons of satellite and ground-based TO measurements in the troposphere layer below 400 hPa for each station are

Table 5. Comparison of TO in the layer below 400 hPa according to FTIR measurements and IKFS-2 (N is the number of comparisons, Δ is the average difference in DU (FTIR minus IKFS-2), and σ is the standard deviation of differences in DU

Station	Notes	*N*	35-0-60		50-0-60		35-0-65		35-0-55		25-0-40	
			Δ	σ	Δ	σ	Δ	σ	Δ	σ	Δ	σ
Eureka	Glacier	282	+3.7	4.2	+3.6	4.2	+3.7	4.2	+3.6	4.2	+3.7	4.2
New Ålesund	Island	120	–0.22	4.4	–0.08	4.4	–0.23	4.4	–0.13	4.4	0.02	4.4
Thule	Glacier	553	+2.1	3.4	+2.2	3.4	+2.1	3.4	+2.0	3.4	+2.3	3.3
Kiruna		491	+1.3	3.9	+1.2	3.8	+1.3	3.9	+1.3	3.8	+1.1	3.9
Harestua		153	–0.55	2.6	–0.47	2.6	–0.6	2.6	–0.41	2.5	–0.65	2.6
St. Petersburg		247	+0.42	3.7	+0.68	3.5	+0.42	3.7	+0.84	3.6	+0.47	3.7
Bremen		129	+0.68	2.5	+0.66	2.6	+0.68	2.5	+0.64	2.7	+0.62	2.7
Zugspitze	Mountains	559	–10.5	3.1	–10.5	3.1	–10.5	3.1	–10.4	3.1	–10.2	2.9
Jungfraujoch	Mountains	441	–12.6	2.1	–12.6	2.1	–12.6	2.1	–12.5	2.0	–12.2	2.0
Toronto TAO		679	+2.2	4.0	+1.9	4.0	+2.2	4.0	+1.9	4.1	+2.3	4.0
Rikubetsu	Island	100	–1.0	3.4	–1.3	3.5	–1.0	3.4	–1.2	3.5	–0.7	3.3
Boulder	Mountains	367	–1.9	2.2	–1.8	2.2	–1.9	2.2	–1.9	2.2	–2.3	2.3
Tsukuba	Island	184	+2.8	4.0	+2.6	3.8	+2.8	4.0	+2.6	4.1	+3.6	3.9
Izaña	Small island	395	–8.7	2.0	–8.2	1.9	–8.7	2.0	–8.2	2.0	–8.8	2.0
Mauna Loa	Small island	659	–8.3	2.5	–8.5	2.3	–8.3	2.5	–8.5	2.1	–8.3	2.3
Altzomoni	Mountains	216	–12.0	2.5	–10.1	2.1	–12.0	2.5	–11.1	2.2	–11.1	2.5
Maido	Small island	342	–5.6	2.2	–5.7	2.3	–5.8	2.2	–5.8	2.1	–5.7	2.4
Wollongong		212	+2.1	2.6	+3.5	2.7	+2.1	2.6	+2.7	2.8	+3.0	2.7
Lauder	Island	940	+1.1	2.0	+1.2	2.1	+1.1	2.0	+1.2	2.1	+1.3	2.0
All		7069		**3.02**		**2.98**		**3.02**		**2.99**		**2.99**

given in Table 5. Note that, for satellite measurements, all data per day falling within a circle with a radius of 200 km from the station were averaged, and for ground-based measurements, daily average values were taken for each day of comparison.

SDDs for different stations differ significantly from each other, which can be explained both by the peculiarities of the location of stations (stability of air masses, altitude, surroundings, etc.) and by different methods for interpreting IR spectroscopic data at different stations. Despite the fact that all stations belong to the same network and are equipped with identical instruments, at each station researchers use their own methods for interpreting spectroscopic data, adapted to the characteristics of the instruments, measurements, and conditions at the stations. Currently, within the framework of the TOAR-II project, a unified interpretation methodology is being introduced, the results of which have not yet been obtained at all stations. MD between ground-based measurements reflect the altitude of the station well; the higher the station (especially for stations located in isolated mountains surrounded by plateaus), the more satellite data overestimate ground-based measurements, due to the fact that the radius around the station includes many measurements with pixel centers at lower altitudes.

As can be seen from Table 5, all ANN variants produce insignificantly different results when comparing satellite TO measurements with independent measurements. Therefore, below we will rely on the choice made above and recommend using the ANN 35-0-55 network to determine TO using IKFS-2 spectral measurements. For this network, we also compared data for all stations, but for the troposphere layer from the surface to 300 hPa. Table 6 shows the averages for all MD stations for two layers of the troposphere for cases where, for comparison, we averaged satellite data within a radius of 100 and 200 km.

As the averaging radius of satellite measurements decreases, the SDD on average does not change noticeably, although, of course, the situations differ at different stations. In general, we can talk about agreement of about 3 DU for all considered comparison options, which is ~15% of TO according to FTIR measurements.

Comparison with Satellite Measurement Data Using the IASI Instrument

We also compared the TO distribution fields obtained from IKFS-2 data for the troposphere up to 300 hPa with data from similar measurements by the

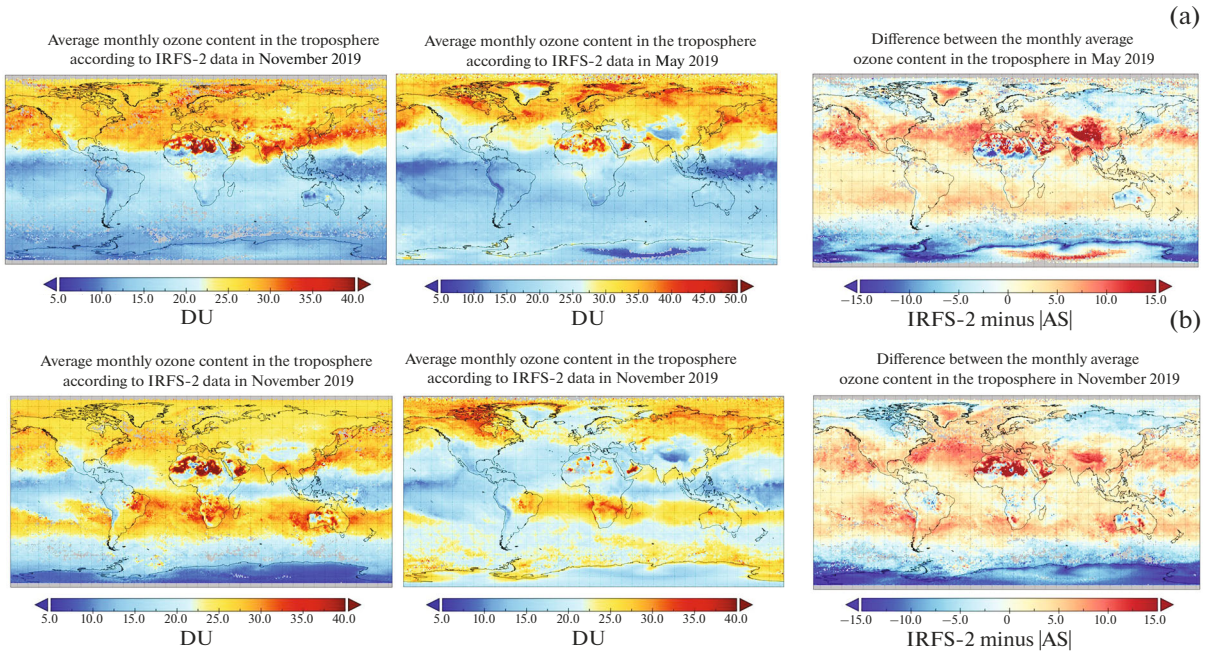

Fig. 2. Spatial distribution of monthly average TO values according to daytime and nighttime measurements of IKFS-2 (left), IASI_LATMOS (middle), and the difference between them (right) in May (a) and November (b) 2019.

IASI satellite instrument, which has characteristics similar to the IKFS-2 instrument data. IASI instruments are located on board polar satellites of the MetOp series (-A, -B, -C), which, like the Meteor-M series spacecraft no. 2, are in sun-synchronous orbits. The IASI data (IASI_LATMOS) used for comparison are based on the interpretation of the measured spectra using the FORLI algorithm of the LATMOS laboratory (Boynard et al., 2018), adopted as an algorithm for the operational processing of IASI spectral data (Daily IASI/Metop-A ULB-LATMOS ozone (O3) L2 product, available on the website https://iasi.aeris-data.fr/catalog). Previously, both IASI and IKFS-2 data were brought to a single grid of 1° longitude and latitude for the entire globe.

In Fig. 2, examples are given of monthly average TO based on IKFS-2 and IASI_LATMOS measurements for May and November 2019. The main features of the TO distribution are repeated across the two data sets. For May 2019 (Fig. 2a), this is a maximum in the Northern Hemisphere with values of ~30–40 DU and a minimum in the south, with a minimum over the Pacific Ocean in the tropics (15–20 DU). For November 2019 (Fig. 2b), the situation is more complex, with a maximum in the Northern Hemisphere, as well as in the Southern, but in the tropical region.

Table 7 shows MD and SDD between IKFS-2 and IASI measurements for six latitude zones. The greatest differences are observed in the polar region of the Southern Hemisphere. Moreover, if the maximum MD occurs in November (9.8 DU), then the maximum SDD occurs in May (5.5 DU). The best agreement between the data in both months occurs in the tropical region of the Southern Hemisphere (0–30 S), where MD and SDD are 2.1–2.2 DU and 2.7–2.9 DU, respectively. The observed values of MD and SDD are smaller in May than in November. The minimum occurs in the polar region of the northern hemisphere (60–90 N) and the middle latitudes of the southern hemisphere (30–60 S) (MD and SDD less than 1 DU).

When comparing our results with various independent data, it should be borne in mind that solving the inverse problem by methods of approximating the training set of pairs (in particular, using ANN) can give good results only if there is a statistical correspondence between the training sample and the atmospheric states during measurements. Since the vast majority of ozone sounding stations are located on land at temperate and high latitudes, it is for land at temperate and high latitudes that the best agreement with independent measurement data should be expected. For example, over the territory of Russia, the differences between IKFS-2

Table 6. Average over 19 stations standard deviations of differences in TO values according to FTIR and IKFS-2 measurements

Troposphere layer to level	Averaging radius of IKFS-2	
	100 km	200 km
300 hPa	2.91 DU	2.95 DU
400 hPa	3.00 DU	2.99 DU

Table 7. Characteristics of the difference in average monthly maintenance according to IKFS-2 and IASI_LATMOS measurements for May and November 2019

Latitudinal zone	MD (May/November 2019), DU	SDD (May/November 2019), DU
60–90 N	–0.7/–0.7	3.2/3.4
30–60 N	3.5/3.7	4.6/3.6
0–30 N	2.6/3.5	4.6/4.5
0–30 S	2.2/2.7	2.1/2.9
30–60 S	–0.5/0.6	3.7/4.1
60–90 S	–6.6/–9.8	5.5/3.9

and IASI data are small. However, there are no ozone sounding stations in deserts. As a result, in Fig. 2 you can see large differences in data over the desert zone of the African continent.

CONCLUSIONS

An algorithm for determining TO based on the spectra of outgoing thermal radiation is proposed. The algorithm was implemented for the Russian IKFS-2 device on board the Meteor-M no. 2 spacecraft. The technique is based on the use of the ANN method and the principal component method. The estimate of the approximation error on the training and test data sets does not exceed 2.8 DU for the layer below 400 hPa and 3.8 DU for the atmospheric layer below 300 hPa.

The satellite TO measurements were validated in the vicinity of 19 stations of the international IRWG-NDACC observational network, located in different regions of the globe. The standard deviations of the differences with the FTIR measurement data ranged from 2 to 4 DU, which is consistent with the results of other authors for similar algorithms. Based on the comparison, the parameters of the optimal ANN were selected to solve the inverse problem of interpreting the spectra measured by IKFS-2. For training, it is optimal to use a set of pairs that includes all IKFS-2 spectra, including cloud ones, with an acceptable discrepancy with measurements at ozone sounding stations of 200 km in space and 24 h in time. In addition to PC spectra, the set of ANN predictors must include the satellite zenith angle, latitude, and day of year of measurement. Optimal ANN structure: 35 PC of the whole spectrum, 0 PC of the ozone band, and 55 HLN.

Examples of the TO distribution fields around the globe are given.

ACKNOWLEDGMENTS

We thank the Planet Research Center for providing access to the results of IKFS-2 spectral measurements. We thank the authors of the programs from the Moscow State University program library for providing free access to the source codes of the programs.

Ground-based FTIR measurement data provided by researchers from stations of the IRWG-NDACC observation network, data available on the website https://www-air.larc.nasa.gov/missions/ndacc/data.html. Homogenized ozone sounding data was provided by the HEGIFTOM working group as part of the TOAR-II project; the data is available on the website https://hegiftom.meteo.be.

The authors thank AERIS for providing access to IASI data, ULB-ATMOS for developing ozone measurement techniques, and Eumetsat/AC SAF for creating the finished product. IASI measurement data is available on the website https://iasi.aeris-data.fr/catalog and FTIR measurement data on the website https://www-air.larc.nasa.gov/missions/ndacc/data.html.

Ground-based spectroscopic measurements at the NDACC St. Petersburg station were carried out using the scientific equipment of the Geomodel resource center at St. Petersburg State University.

FUNDING

This research was funded by the Russian Science Foundation, grant no. 23-27-00166, https://rscf.ru/project/23-27-00166.

CONFLICT OF INTEREST

The authors of this work declare that they have no conflicts of interest.

REFERENCES

Amann, M., Derwent, D., Forsberg, B., Hänninen, O., Hurley, F., et al., 2008, *Health Risks of Ozone From Long-Range Transboundary Air Pollution*, World Health Organization Regional Office for Europe, 2008. https://apps.who.int/iris/handle/10665/326496.

Andreev, V.V., Arshinov, M.Yu., Belan, B.D., Belan, S.B., Davydov, D.K., Demin, V.I., Dudorova, N.V., Elansky, N.F., Zhamsueva, G.S., Zayakhanov, A.S., Ivanov, R.V., Ivlev, G.A., Kozlov, A.V., Konoval'tseva, L.V., Korenskii, M.Yu., et al., Tropospheric ozone concentration in Russia in 2022, *Atmos. Oceanic Opt.*, 2023, vol. 36, no. 6, pp. 741–757. https://doi.org/10.1134/S1024856023060040

Antokhin, P.N., Arshinov, M.Yu., Belan, B.D., Davydov, D.K., Zhidovkin, E.V., Ivlev, G.A., Kozlov, A.V., Kozlov, V.S., Panchenko, M.V., Penner, I.E., Pestunov, D.A., Simonenkov, D.V., Tolmachev, G.N., Fofonov, A.V., Shamanaev, V.S., and Shmargunov, V.P., Optik- É AN-30 aircraft laboratory for studies of the atmospheric composition, *J. Atmos. Oceanic Technol.*, 2012, vol. 29, no. 1, pp. 64–75.

Asmus, A.A., Zagrebaev, V.A., Makridenko, L.A., Milekhin, O.E., Solovyev, V.I., Uspenskii, A.B., Frolov, A.V., and Khailov, M.N., Meteorological satellites based on Meteor-M polar orbiting platform, *Russ. Meteorol. Hydrol.*, 2014, no. 12, pp. 787–794.

Asmus, V.V., Timofeyev, Y.M., Polyakov, A.V., et al., Atmospheric temperature sounding with the Fourier spectrometer, *Izv., Atmos. Ocean. Phys.*, 2017, vol. 53, pp. 428–432. https://doi.org/10.1134/S0001433817040028

Belan, B.D., Ancellet, G., Andreeva, I.S., Antokhin, P.N., Arshinova, V.G., Arshinov, M.Y., Balin, Y.S., Barsuk, V.E., Belan, S.B., Chernov, D.G., Davydov, D.K., Fofonov, A.V., Ivlev, G.A., Kotel'nikov, S.N., Kozlov, A.S., et al., Integrated airborne investigation of the air composition over the Russian sector of the Arctic, *Atmos. Meas. Tech.*, 2022, vol. 15, no. 13, pp. 3941–3967.

Boynard, A., Hurtmans, D., Garane, K., Goutai, F., Hadji-Lazaro, J., Koukouli, M.E., Wespes, C., Vigouroux, C., Keppens, A., Pommereau, J.-P., Pazmino, A., Balis, D., Loyola, D., Valks, P., Sussmann, R., et al., Validation of the IASI FORLI/EUMETSAT ozone products using satellite (GOME-2), ground-based (Brewer-Dobson, SAOZ, FTIR) and ozonesonde measurements, *Atmos. Meas. Tech.*, 2018, vol. 11, no. 9, pp. 5125–5152.

Cuesta, J., Eremenko, M., Liu, X., Dufour, G., Cai, Z., Hopfner, M., von Clarmann, T., Sellitto, P., Foret, G., Gaubert, B., Beekmann, M., Orphal, J., Chance, K., Spurr, R., and Flaud, J.-M., Satellite observation of lowermost tropospheric ozone by multispectral synergism of IASI thermal infrared and GOME-2 ultraviolet measurements over Europe, *Atmos. Chem. Phys.*, 2013, vol. 13, no. 19, pp. 9675–9693.

Dorokhov, V., Yushkov, V., Makshtas, A., Ivlev, G., Tereb, N., Savinykh, V., Shepelev, D., Nakajima, H., McElroy, C.T., Tarasick, D., Goutail, F., Pommereau, J.-P., and Pazmino, A., Brewer, SOAZ and ozonesonde observations in Siberia, *Atmosphere-Ocean*, 2013, vol. 51, no. 3, pp. 14–18.

Dufour, G., Eremenko, M., Griesfeller, A., Barret, B., LeFlochmoen, E., Clerbaux, C., Hadji-Lazaro, J., Coheur, P.-F., and Hurtmans, D., Validation of three different scientific ozone products retrieved from IASI spectra using ozonesondes, *Atmos. Meas. Tech.*, 2012, vol. 5, no. 3, pp. 611–630.

Elansky, N.F., Golitsyn, G.S., Crutzen, P.J., Belikov, I.B., Brenninkmmeijer, C.A.M., and Skorokhod A.I., Observations of the atmospheric composition over Russia: TROICA experiments, *Izv., Atmos. Ocean. Phys.*, 2021, vol. 57, no. 1, pp. 72–90.

Forster, P., Storelvmo, T., Armour, K., Collins, W., Dufresne, J.-L., Frame, D., Lunt, D.J., Mauritsen, T., Palmer, M.D., Watanabe, M., Wild, M., and Zhang, H., The Earth's energy budget, climate feedbacks, and climate sensitivity, in *Climate Change 2021: The Physical Science Basis. Contribution of Working Group I to the Sixth Assessment Report of the Intergovernmental Panel on Climate Change*, New York: Cambridge University Press, 2021, ch. 7, pp. 923–1054. https://www.ipcc.ch/report/ar6/wg1/downloads/report/IPCC_AR6_WGI_Chapter07.pdf.

Garkusha, A.S., Polyakov, A.V., Timofeev, Yu.M., and Virolainen, Ya.A., Determination of the total ozone content from data of satellite IR Fourier-spectrometer, *Izv., Atmos. Ocean. Phys.*, 2017, vol. 53, no. 4, pp. 433–440. https://doi.org/10.1134/S0001433817040041

Gaudel, A., Cooper, O.R., Ancellet, G., Barret, B., Boynard, A., Burrows, J.P., Clerbaux, C., Coheur, P.-F., Cuesta, J., Cuevas, E., Doniki, S., Dufour, G., Ebojie, F., Foret, G., Garcia, O., et al., Tropospheric ozone assessment report: Present-day distribution and trends of tropospheric ozone relevant to climate and global atmospheric chemistry model evaluation, *Elementa: Sci. Anthropocene*, 2018, vol. 39, no. 6.

Golovin, Y.M., Zavelevich, F.S., Nikulin, A.G., Kozlov, D.A., Monakhov, D.O., Kozlov, I.A., Arkhipov, S.A., Tselikov, V.A., Romanovskii, A.S., Spaceborne infrared Fourier-transform spectrometers for temperature and humidity sounding of the Earth's atmosphere, *Izv., Atmos. Ocean. Phys.*, 2014, vol. 50, no. 9, pp. 1004–1015.

Hubert, D., Heue, K.-P., Lambert, J.-C., Verhoelst, T., Allaart, M., Compernolle, S., Cullis, P.D., Dehn, A., Felix, C., Johnson, B.J., Keppens, A., Kollonige, D.E., Lerot, C., Loyola, D., Maata, M., et al., TROPOMI tropospheric ozone column data: Geophysical assessment and comparison to ozonesondes, GOME-2B and OMI, *Atmos. Meas. Tech.*, 2021, vol. 14, no. 12, pp. 7405–7433.

IPCC: Climate Change 2013: The Physical Science Basis. Contribution of Working Group I to the Fifth Assessment Report of the Intergovernmental Panel on Climate Change, Stocker, T.F., Qin, D., Plattner, G.-K., Tignor, M., Allen, S.K., Boschung, J., Nauels, A., Xia, Y., Bex, V., and Midgley, P.M., Eds., New York: Cambridge University Press, 2013. Karol', I.L., Kiselev, A.A., Genikhovich, E.L., and Chicherin, S.S., Short-lived radiation-active impurities in the atmosphere and their role in modern climate changes, *Tr. Gl. Geofiz. Obs. im. A.I. Voeikova*, 2012, no. 567, pp. 5–82.

Matvienko, G.G., Babushkin, P.A., Bobrovnikov, S.M., Borovoi, A.G., Bochkovskii, D.A., Galileiskii, V.P., Grishin, A.I., Dolgii, S.I., Elizarov, A.I., Kokarev, D.V., Konoshonkin, A.V., Kryuchkov, A.V., Kustova, N.V., Nevzorov, A.V., Marichev, V.N., et al., Laser and optical sensing of the atmosphere, *Atmos. Oceanic Opt.*, 2020, vol. 33, no. 1, pp. 51–68.

Polyakov, A.V., The method of artificial neural networks in retrieving vertical profiles of atmospheric parameters, *Atmos. Oceanic Opt.*, 2014, vol. 27, no. 3, pp. 247–252.

Polyakov, A., Virolainen, Y., Nerobelov, G., Timofeyev, Y., and Solomatnikova, A., Total ozone measurements using IKFS-2 spectrometer aboard Meteor-M N2 satellite in 2019–2020, *Int. J. Remote Sens.*, 2021, vol. 42, no. 22, pp. 8709–8733.

Polyakov, A.V., Timofeev, Yu.M., and Virolainen, Ya.A., Using artificial neural networks in the temperature and humidity sounding of the atmosphere, *Izv., Atmos. Ocean. Phys.*, 2014, vol. 50, no. 3, pp. 330–336.

Polyakov, A., Virolainen, Y., Nerobelov, G., Kozlov, D., and Timofeyev, Y., Six years of IKFS-2 global ozone total column measurements, *Remote Sens.*, 2023, vol. 15, p. 2481. https://doi.org/10.3390/rs15092481

Rublev, A.N., Uspenskii, A.B., Trotsenko, A.N., Udalova, T.A., and Volkova, E.V., Detecting and evaluating the cloud amount according to atmospheric high spectral resolution IR sounding data, *Issled. Zemli Kosmosa*, 2004, no. 3, pp. 43–51.

Stanek, L.W., Brown, J.S., Stanek, J., Gift, J., and Costa, D.L., Air pollution toxicology: A brief review of the role of the science in shaping the current understanding of air pollution health risks, *Toxicol. Sci.*, 2011, vol. 120, no. 1, pp. S8–S27. https://doi.org/10.1093/toxsci/kfq367

Tarasick, D., Galbally, I.E., Cooper, O.R., Schultz, M.G., Ancellet, G., Leblanc, T., Wallington, T.J., Ziemke, J., Liu, X., Steinbacher, M., Staehelin, J., Vigouroux, C., Hannigan, J.W., Garcia, O., Foret, G., et al., Tropospheric ozone assessment report: Tropospheric ozone from 1877 to 2016, observed levels, trends and uncertainties, *Elementa: Sci. Anthropocene*, 2019, vol. 39, no. 7. https://doi.org/10.1525/elementa.376

Tarasick, D.W., Smit, H.G.J., Thompson, A.M., Morris, G.A., Witte, J.C., Davies, J., et al., Improving ECC ozonesonde data quality: Assessment of current methods and outstanding issues, *Earth Space Sci.*, 2021, vol. 8, no. 3. https://doi.org/10.1029/2019EA000914

Timofeyev, Y.M., Uspensky, A.B., Zavelevich, F.S., Polyakov, A.V., Virolainen, Y.A., Rublev, A.N., Kukharsky, A.V., Kiseleva, J.V., Kozlov, D.A., Kozlov, I.A., Nikulin, A.G., Pyatkin, V.P., and Rusin, E.V., Hyperspectral infrared atmospheric sounder IKFS-2 on "Meteor-M" No. 2: Four years in orbit, *J. Quant. Spectrosc. Radiat. Transfer*, 2019, vol. 238, p. 106579. https://doi.org/10.1016/j.jqsrt.2019.106579

Vigouroux, C., Blumenstock, T., Coffey, M., Errera, Q., Garcia, O., Jones, N.B., Hannigan, J.W., Hase, F., Liley, B., Mahieu, E., Mellqvist, J., Notholt, J., Palm, M., Persson, G., Schneider, M., et al., Trends of ozone total columns and vertical distribution from FTIR observations at eight NDACC stations around the globe, *Atmos. Chem. Phys.*, 2015, vol. 15, no. 6, pp. 2915–2933.

Virolainen, Ya.A., Ionov, D.V., and Polyakov, A.V., Analysis of long-term measurements of tropospheric ozone at the St. Petersburg State University observational site in Peterhof, *Izv., Atmos. Ocean. Phys.*, 2023a, vol. 59, no. 3, pp. 287–295. https://doi.org/10.1134/S000143382303009X

Virolainen, Ya.A., Nerobelov, G.M., and Polyakov, A.V., Comparison of satellite and ground-based measurements of tropospheric ozone columns in the vicinity of St. Petersburg, *Izv., Atmos. Ocean. Phys.*, 2023b, vol. 59, no. 4, pp. 411–420. https://doi.org/10.1134/S000143382304014X

Virolainen, Y., Nerobelov, G., Polyakov, A., and Akishina, S., Comparison of satellite and ground-based measurements of tropospheric ozone, in *Proc. SPIE–Int. Soc. Opt. Eng., 29th International Symposium on Atmospheric and Ocean Optics: Atmospheric Physics*, 2023c, vol. 12780, p. 127804X. https://doi.org/10.1117/12.2688764.short.

Wu, S., Mickley, L.J., Jacob, D.J., Logan, J.A., Yantosca, R.M., and Rind, D., Why are there large differences between models in global budgets of tropospheric ozone?, *J. Geophys. Res.*, 2007, vol. 112, p. D05302.

Young, P.J., Archibald, A.T., Bowman, K.W., Lamarque, J.-F., Naik, V., Stevenson, D.S., Tilmes, S., Voulgarakis, A., Wild, O., Bergmann, D., Cameron-Smith, P., Cionni, I., Collins, W.J., Dalsoren, S.B., Doherty, RM., et al., Pre-industrial to end 21st century projections of tropospheric ozone from the Atmospheric Chemistry and Climate Model Intercomparison Project (ACCMIP), *Atmos. Chem. Phys.*, 2013, vol. 13, no. 4, pp. 2063–2090.

Ziemke, J.R., Chandra, S., Duncan, B.N., Froidevaux, L., Bhartia, P.K., Levelt, P.F., and Waters J.W., Tropospheric ozone determined from Aura OMI and MLS: Evaluation of measurements and comparison with the global modeling initiative's chemical transport model, *J. Geophys. Res.*, 2006, vol. 111, p. D19303. https://doi.org/10.1029/2006JD007089

Zvyagintsev, A.M., Spatiotemporal variability of ozone in the troposphere, *Doctoral (Phys.-Math.) Dissertation*, Moscow, 2013.

Publisher's Note. Pleiades Publishing remains neutral with regard to jurisdictional claims in published maps and institutional affiliations.

AI tools may have been used in the translation or editing of this article.